Archives of Hydro-Engineering and Environmental Mechanics
Vol. 58 (2011), No. 1–4, pp. 47–64
DOI: 10.2478/v10203-011-0003-8

Application of SEM to Analysis of Permeability Coefficient of Cohesive Soils

Tomasz Kozłowski, Katarzyna Kurpias-Warianek, Łukasz Walaszczyk

Department of Geotechnical and Water Engineering, Kielce University of Technology, Poland
e-mail: tomkoz@tu.kielce.pl

(Received March 13, 2011; revised September 12, 2011)

Abstract

A series of experiments on samples of five clayey soils gave evidence that cyclic freezing and thawing significantly affects the permeability coefficient. An attempt to analyze these changes on base of the Scanning Electron Microscopy SEM photographs of microstructures has been made. A simplistic equation (Eq. 11) has been drawn, describing the permeability coefficient as a function of hydraulic radius and pore area. An approach to determine the permeability coefficient by Eq. (11) on base of SEM photographs, in which the pores were identified manually, yielded results comparable to the Falling Head Test (FHT). However, since the identification of pores in SEM photographs seems the critical point of the method, the Numerical Image Analysis (NIA) has been applied. The procedure of finding the optimum threshold T_{opt} has been described, based on minimization of the deviation $\Delta k_{i,j}$, calculated as the absolute value of the difference $k_{SEM,i,j}$ and $k_{FHT,j}$, i.e. the permeability coefficients determined by the SEM analysis and FHT, respectively. It has been proved that the optimum threshold values can be described as a function of image parameters, i.e. mean grey level L_{mean} and standard deviation σ_n.

Key words: cohesive soils, permeability coefficient, SEM, NIA, cyclic freezing and thawing

Notations

A – area of the whole of analyzed region in SEM photograph (μm),
a – cross-section of pipe (cm^2),
A – cross-section of soil sample (cm^2),
A_i – cross-section area of pore i (μm),
FHT – Falling Head Test,
h_1 – height of water table at time t_0 (cm),
h_2 – height of water table at time t (cm),
i – hydraulic gradient,
k – local value of the permeability coefficient in analyzed region (m/s),

k_{10} – permeability coefficient at 10°C (m/s),
k_{FHT} – permeability coefficient determined by use of the Falling Head Test (m/s),
k_{SEM} – permeability coefficient determined by use of SEM (m/s),
Δk – absolute value of the difference k_{SEM} and k_{FHT},
l – height of soil sample (cm),
$L_{\max}$ – maximum gray level (image parameter),
L_{mean} – mean gray level (image parameter),
L_{med} – median gray level (image parameter),
$L_{\min}$ – minimum gray level (image parameter),
p – the p-value,
Q – total flow rate (m^3/s),
R – correlation coefficient,
$R_{h,i}$ – hydraulic radius of pore i (μm),
R_i – radius of circular cross-section of a duct i (m),
SEM – Scanning Electron Microscopy,
t – time (s),
T – threshold value (image parameter),
$T_{\min}$ – minimal threshold value (image parameter),
T_{opt} – optimum threshold value (image parameter),
U_i – perimeter of pore i (μm),
v – flow velocity (m/s),
γ – volumetric weight of water (N/m^3),
μ – dynamic viscosity of water (Ns/m^2),
σ_n – standard deviation or contrast (image parameter).

1. Introduction

Results reported by many authors give evidence that cyclic freezing and thawing (CFT) of cohesive soils leads to changes in many geotechnical parameters, such as limits of consistency (Aoyama et al 1985, Yong et al 1985), permeability coefficient (Chamberlain and Gow 1979, Nagasawa and Umeda 1985, Baykal and Türe 1998, Viklander and Eigenbrod 2000), shear resistance (Ogata et al 1985, Aoyama et al 1985, Baykal and Türe 1998, Wang et al 2007) and others. The direct cause of these changes are modifications of microstructure as an effect of the CFT (Skarzynska 1980, 1985, Yong et al 1985, Kujala and Laurinen 1989, Stepkowska and Skarzynska 1989, Kumor 1989, Hohmann-Porebska 2002). From among many quite complicated methods used in the investigation and description of microstructural soil parameters, probably most information is given by Scanning Electron Microscopy (SEM). Examination of the SEM images involves both qualitative and quantitative analysis of pore space, the latter determining porosity, total and average pore area, average pore perimeter, average pore diameter and the

so called morphometric parameters, describing the shape of the pores (Sergeev et al 1984). The hypothesis that there is a strict relationship between the pore space parameters and the permeability coefficient seems to be very reasonable. However, there is practically a lack of useful methods able to describe the permeability coefficient as a function of microstructure. Such a method would be particularly useful in cases when a comparison between many different samples should be done or the available samples are too small for laboratory investigation. In the paper, an attempt to determine a relationship making it possible to determine local values of the permeability coefficient on base of the SEM data is presented. The method has been applied to examine changes in the permeability coefficient in five natural cohesive soils due to cyclic freezing and thawing. A verification has been done by comparison with results of conventional Falling Head Test (FHT).

2. Materials

Five natural clayey (cohesive) soils were used in the experiment. All the samples were obtained from Kielce, Poland, at about 3.0–7.0 m depth, well below the frost penetration depth in that region. The initial values of soil parameters are given in Table 1. In this paper, the arbitrary letter symbols A ÷ E have been assigned to the soils. The plasticity characteristics were determined by use of normal, widely known procedures (the Casagrande's cup device and the rolling test, for w_L and w_P respectively). The specific surface area determinations were based on results of sorption of water according to Stepkowska (1977).

The soils are characterized in Table 1. In terms of the Unified Soil Classification System (USCS) the soils A, B, C and D are "lean clays" (CL) and the soil E can be named as "fat clay" (CH) (Das 1985).

Table 1. Soil properties

No.	Classification by USCS		Water content	Plasticity limit	Liquidity limit	Specific surface area	Fraction of particles		
	Group	Name	%	%	%	m^2/g	< 0.002 mm	0.002–0.05 mm	0.05–2 mm
1	CL	Slc	21.71±1.74	17.10±0.58	42.32±2.84	63.80±2.66	17	31	51
2	CL	Slc	18.11±1.18	14.16±0.86	32.50±3.00	60.80±2.20	14	34	51
3	CL	Slc	30.20±2.41	10.23±1.24	48.80±2.22	157.92±1.86	18	47	35
4	CL	Slc	19.56±0.74	14.80±0.62	28.90±1.77	57.10±2.36	13	29	55
5	CL	Slc	23.51±2.60	10.76±1.73	26.35±2.07	49.80±3.18	12	30	57

Slc = Sandy lean clay

3. Experimental Procedures

3.1. Cyclic Freezing and Thawing (CFT)

The cyclic freezing and thawing (CFT) was accomplished both in the closed and the open system. The process of CFT in the closed system made impossible any

change in mass of a sample, both as a result of a water uptake from beneath during freezing and an evaporation during thawing. Such a system simulated the situation where a low permeability soil underwent freezing without access to a free water source and thawed subsequently without any drainage facility (Yong et al 1985). All soil samples were subjected to freezing and thawing in cylindrical steel containers of 65 mm in diameter and 220 mm height installed in a thick styrofoam block placed in a freezing chamber. Each sample was preserved against any moisture loss by putting an aluminium film cover on the top followed by flooding with liquid paraffin. Special laboratory equipment enabled us to create conditions corresponding with the open system. Steel tubes of dimensions identical to those used in the closed system experiments were placed in holes in a thick styrofoam block. Water uptake from beneath was accomplished by mounting ceramic filters at the bottom of the tubes. The filters were submerged in a thermostated water container. The average temperature of water in the container was maintained at about +5°C. A stable level of water was assured by a float-valve controlling water flow from a container outside the freezing chamber. Thus both in the case of the closed and the open system freezing occured from above, analogically to natural conditions. Freezing was induced by lowering the temperature to −25°C for 24 hours and subsequent thawing was activated in a climatic chamber at 20°C for 24 hours. After a sample was subjected to the required number of freeze-thaw cycles (i.e. 1, 2, 5 and 10), it was tested to determine any change in the initial properties.

3.2. Scanning Electron Microscopy (SEM)

The SEM experiments were carried out on air dried samples of 8–10 mm in diameter. Such a sample preparation in the case of soils in which contacts between structural units are stable, usually phase ones, lead to practically no microstructural changes during drying (Grabowska-Olszewska 1990). It was assumed that the soils used in the investigation, as not being composed of large quantities of clay fraction, can be numbered among such a category. The sample surface was obtained by chipping off (Grabowska-Olszewska 1998). The samples were broken and covered by a layer of gold of approx. 40 nm to prevent electrization. The observation of the surface of the fracture was made by scanning microscope JEOL JSM-5400 with applying voltage of 10 kV. As a rule, only surfaces parallel to stratification were examined. The photographs were taken at two magnifications: x1000 and x5000. The lesser magnification images were used to determine the quantitative pore space parameters, while the x5000 magnification images made it possible to characterize the microstructure qualitatively, among other things to determine the types of contacts.

In this study, samples of soils not subjected to freezing (N) and subjected to one cycle of CFT in the closed (C) and the open (O) system were used, which

yielded 15 different groups (5 soils × 3 systems: N, O, C). The total number of such samples were 50, hence the groups under investigation were unequal.

3.3. Falling Head Test (FHT)

The permeability coefficient was determined in laboratory by the widely known falling head test (FHT). The principle of the method is summarized in Fig. 1. The water table h in the pipe is a function of time $h(t)$. Initially ($t = t_0$) the water table is h_0. V is the volume of water that leaves the tube during Δt, while the water table drops from h_0 to $h(t_0 + \Delta t)$. It can be easily proved that the permeability coefficient can be obtained as

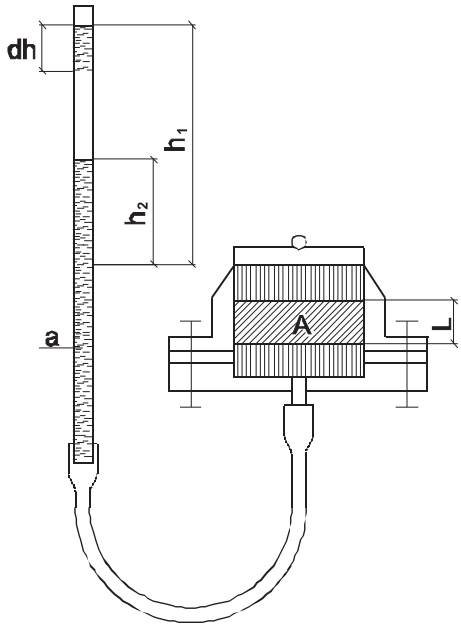

Fig. 1. The principle of the Falling Head Test method

$$k = \frac{a \cdot l}{A \cdot t} \ln \frac{h_1}{h_2}, \tag{1}$$

where:

- A – cross-section of soil sample, cm^2,
- a – cross-section of pipe, cm^2,
- t – time, s,
- l – height of soil sample, cm,
- h_1 – height of water table at time t_0, cm,
- h_2 – height of water table at time t, cm.

As in the case of SEM, the experiments were carried out on samples not subjected to freezing (N) and subjected to one cycle of CFT in the closed (C) and the open (O) system. The obtained results gave evidence that CFT significantly affects the permeability coefficient (*vide* Fig. 6 in the next section). It seems that the initial value of the permeability coefficient can be either decreased or increased by CFT and it has been proved that the nature of these changes can be related to the plasticity and liquidity indices of soils. A detailed analysis will be presented elsewhere.

4. Determining Local Values of the Permeability Coefficient on Base of Pore Space Parameters

4.1. Derivation of Equation for the Permeability Coefficient

In Fig. 2, a flat segment of a cohesive soil, comprehended as a system of ducts having variable cross sectional areas A_i, is shown. The area of the segment is A. In the case of filtration, the total flow rate Q perpendicularly to the segment equals the sum of elementary flow rates Q_i through the individual ducts:

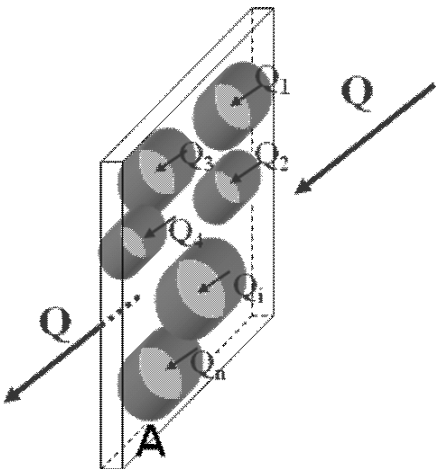

Fig. 2. The total flow rate Q perpendicularly to a flat segment of cohesive soil as the sum of the elementary flow rates Q_i through individual ducts

$$Q = \sum Q_i. \tag{2}$$

From the Darcy's law

$$v = k \cdot i \tag{3}$$

one can obtain for the whole of the segment

$$Q = k \cdot i \cdot A, \tag{4}$$

where:

- v – flow velocity, m/s,
- k – local value of the permeability coefficient in the region of the segment, m/s,
- i – hydraulic gradient
- Q – total flow rate, m^3/s.

Substituting Eq. (2) to Eq. (4) yields:

$$\sum Q_i = k \cdot i \cdot A. \tag{5}$$

Next, a flow rate Q_i through an elementary duct i can be expressed, by use of the Hagen-Poiseuille equation describing flow through a tubular duct (Landau and Lifshitz 1987), as

$$Q_i = \frac{\gamma \cdot i \cdot A_i \cdot R_i^2}{8\mu}, \tag{6}$$

where:

- γ – volumetric weight of water, N/m^3,
- R_i – radius of circular cross-section of a duct i, m,
- μ – dynamic viscosity of water, Ns/m^2.

After substituting Eq. (6) into Eq. (5) the following relationship is yielded

$$\sum \frac{\gamma \cdot i \cdot A_i \cdot R_i^2}{8\mu} = k \cdot i \cdot A, \tag{7}$$

from which, after rearranging, the equation describing local value of the permeability coefficient is obtained:

$$k = \frac{\gamma \sum A_i \cdot R_i^2}{8\mu \cdot A}. \tag{8}$$

Taking into consideration the relationship between the radius R_i of a duct having circular cross-section and the hydraulic radius of a duct having any cross-section shape

$$R_i = 2R_{h,i}, \tag{9}$$

the equation finally assumes the following form:

$$k = \frac{\gamma \sum A_i \cdot R_{h,i}^2}{2\mu \cdot A}. \tag{10}$$

After substituting to Eq. (10) the value of dynamic viscosity of water at 10°C ($\mu = 0.0013077$ Ns/m^2) and, at the same temperature, the volumetric weight of water ($\gamma = 9997$ N/m^3), the equation is obtained, enabling one to estimate the permeability coefficient on base of pore space parameters taken from SEM photograph:

$$k_{10} = \frac{\sum A_i \cdot R_{h,i}^2}{A} \cdot 3.82235 \cdot 10^{-6}, \tag{11}$$

where:

A_i – cross-section area of pore i, μm,
$R_{h,i}$ – hydraulic radius of pore i, μm,
A – area of the whole of analyzed region, μm,
k – permeability coefficient at 10°C, m/s.

The hydraulic radius is defined as

$$R_{h,i} = \frac{A_i}{U_i}, \tag{12}$$

where U_i is perimeter of pore i, μm.

4.2. Identification of Pores in SEM Photograph

Applying Eq. (11) to estimate local values of the permeability coefficient needs to solve the problem of identification of pores in SEM photograph. At first approximation, the pores were identified manually, as distinctly darker areas. For pores separated in this manner, their areas A_i and perimeters U_i were determined automatically by use of the AutoCad software. Next, the data were introduced into the Microsoft Excel and the hydraulic radii $R_{h,i}$ according to Eq. (12) and the permeability coefficient according to Eq. (11) were calculated.

In Fig. 6, the average values of the permeability coefficient obtained by analysis of the SEM photographs for each of 15 groups (5 soils × 3 freezing systems) are compared with the values obtained by the FHT method. It can be seen that estimation of the permeability coefficient by analysis of the SEM photographs yields results not very scattered from those obtained indirectly (FHT). The extreme differences are not greater than one order of magnitude, which can be accepted as a satisfying result compared with the possible variation of the soil permeability coefficient, which ranged from 10^{-3} to 10^{-9} m/s. Moreover, in six cases (for the general number 15) the agreement is almost ideal. Such results could appear surprising in the face of the fact that the comparison involved the FHT data obtained for 3D macroscopic samples on the one hand and the microscopic SEM data, actually

2D ones, on the other. However, it seems that an equation like Eq. 11 expresses a statistical "permeability potential" of a pore medium and, although cannot be comprehended as a proper theoretical description, it is able to yield reasonable solutions.

Although the above results can be admitted to be satisfying and confirming the correctness of the model described by Eq. (11), the basic weakness of the method in this version is the identification of pores. Probably, at least in a part of cases, pores are incorrectly identified. To eliminate this disadvantage, an attempt to apply the Numerical Image Analysis (NIA) has been undertaken.

The SEM photographs are represented as grayscale digital images, in which the value of each pixel is a single sample, that is, it carries the full (and only) information about its intensity. Typically, the images are stored with 8 bits per sampled pixel, which allows 256 different intensities (i.e., shades of gray) to be recorded. Thus, the intensity of a pixel is expressed within a given range between a minimum and a maximum, inclusive. This range is represented in an abstract way as a range from 0 (black) and 256 (white), with any fractional values in between.

In SEM photograph of a clayey soil, darker areas correspond to pores and whiter areas – to mineral particles. Hence, a phenomenological analysis of such an image enables one to distinguish between pores and particles with a probability dependent on intensity of individual elements. The elements with intensity approximately equal to 0 are undoubtedly pores, while elements very bright, with intensity approximately near to 256, can be most certainly classified as particles. However, regions of pixels having intermediate values of intensity make serious problems. In such cases, a "manual" categorization of an element among pores or particles can prove strongly controversial. Instead, the numerical image analysis NIA allows an image segmentation method called thresholding. Individual pixels in a grayscale image are marked as "object" pixels if their value of intensity is less than some threshold value (assuming an object to be darker than the background, as in the case of pores) and as "background" pixels otherwise. This way the error connected with manual selection, based on subjective and partially intuitive classification of intensity, is eliminated.

In this study, the numerical image analysis was carried out by use of the UTH-SCSA ImageTool software made by Health Science Center at Texas University, San Antonio.

The key parameter in thresholding is obviously the choice of the proper threshold. Pores identified at various thresholds will yield different values of the permeability coefficient (Fig. 3). There is only one optimal value of threshold identifying pores most properly. Several different methods for choosing the threshold exist. The simplest method would be to choose the mean or median value, the rationale being that if the object pixels are brighter than the background, they should also be brighter than the average. In a noiseless image with uniform background and object values, the mean or median will work as the threshold, however generally

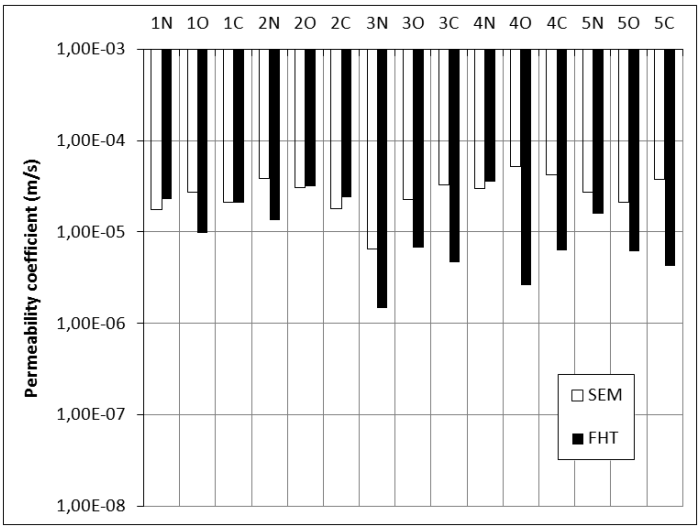

Fig. 3. Comparison of the average values of the permeability coefficient obtained by analysis of the SEM photographs (pores identified manually) and the values obtained by the FHT method in five soils frozen in three freezing systems: N – non-frozen, O – open system, C – closed system

speaking, this will not be the case. A more sophisticated approach might be to create a histogram of the image pixel intensities and use the valley point as the threshold. The histogram approach assumes that there is some average value for the background and object pixels, but that the actual pixel values have some variation around these average values. However, many image histograms do not have clearly defined valley points.

The alternative method of thresholding, proposed in this paper, could find use wherever possible to determine a "threshold function", describing the values of the threshold in relation to image parameters, on base of independent experimental data. In this study, the role of such an independent investigation is played by the Falling Head Test.

The principle of the method is presented on the flow chart in Fig. 4:

1. For a sample j, the initial threshold value is assumed as equal to a minimal value $T_{\min}$, as the lower limit of a set of values giving good fitting to experimental data for individual samples in the population. In this study, $T_{\min}$ was equal to 40 but when no information is available, it could equal zero.
2. For a sample j in approach i, the next threshold value is assumed, greater by one than the previous. For each value of $T_{i,j}$, the permeability coefficient $k_{SEM,i,j}$ is calculated by use of Eq. (11).
3. The deviation $\Delta k_{i,j}$ is calculated as the absolute value of the difference $k_{SEM,i,j}$ and $k_{FHT,j}$, i.e. the permeability coefficient determined by the SEM analysis and the falling head test, respectively.

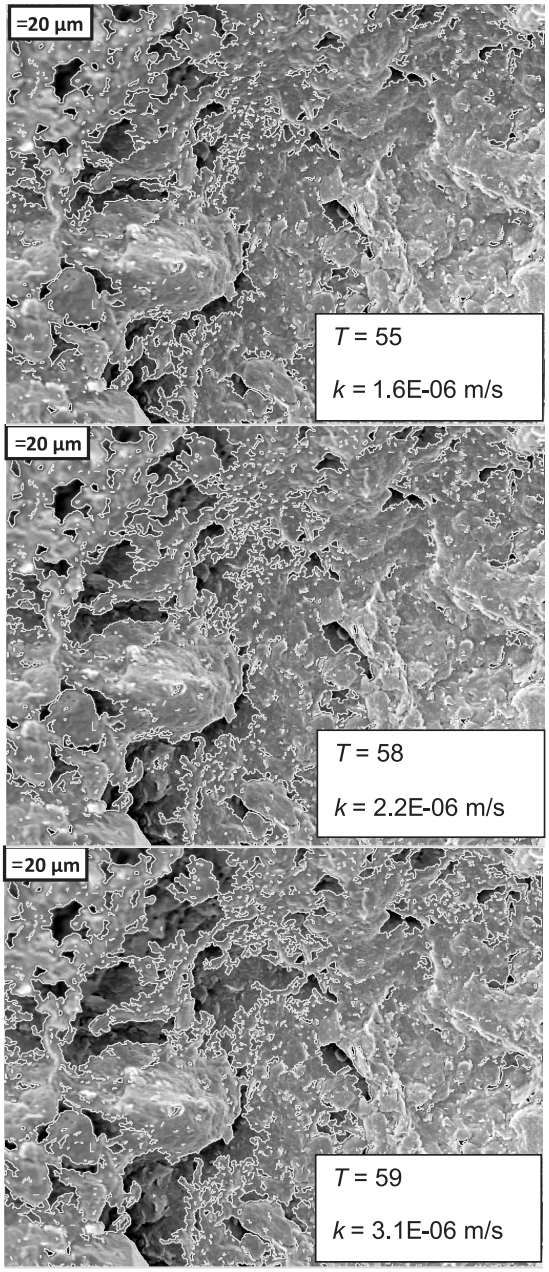

Fig. 4. The permeability coefficient determined at three different threshold values T (sample: soil 1, frozen in open system)

4. If the deviation calculated in the above manner is less than the previous one, the optimum threshold value $T_{opt,j}$ is assumed as equal to the present threshold value $T_{i,j}$ and then, after increasing the value of i, the procedure is repeated from the step 2. Alternatively, if the present deviation is not less than the previous one, the procedure is finished for the sample j and the next sample $j + 1$ is begun to be analyzed, since it is assumed that the subsequent increment of the threshold value would only result in increase of the deviation (in other words, the function $\Delta k_{i,j} = f(T_{i,j})$ has only one extreme for given j). Thereby, the threshold value determined in previous approach remains the optimum threshold value $T_{opt,j}$ for the sample j.

As the result of the above procedure, a set of optimum threshold values has been obtained:

$$A = \{T_{opt,j} = T_{i,j} : \Delta k_{i,j} = \min\}. \tag{13}$$

In Fig. 5, the plot of the k_{SEM} vs. k_{FHM} is presented, the former being determined at the optimum threshold value. It is easy to notice that there is a very good agreement between values obtained by SEM analysis and those measured indirectly, which is confirmed by the very high value of the correlation coefficient ($R = 0.982$). The agreement is significantly better than that observed for the values of the permeability coefficient determined by SEM when pores were determined manually (Fig. 6).

However, for obvious reasons, the presented method of analysis of SEM photographs still does not satisfy criteria of a universal method, because analysis of each sample needs an independent laboratory data as a standard. Trying to solve the problem, factors affecting the optimal values of threshold were searched for. Hence, it has been assumed that there are measurable image parameters determining pores in an optimal manner from the point of view of estimating the permeability coefficient. The initial stage of testing such a hypothesis was analysis of correlation coefficient of T_{opt} with all the image parameters provided by the ImageTool software. The values of $R \approx 0$ for minimum gray level $L_{\min}$, $R = 0.42$ for mean gray level L_{mean}, $R = -0.22$ for median gray level L_{med}, $R = 0.09$ for mode gray level L_{mod}, $R = -0.16$ for maximum gray level $L_{\max}$ and $R = 0.66$ for standard deviation σ_n were obtained. Only the correlations with L_{mean} and σ_n were significant at $p < 0.05$. From a practical point of view, these parameters refers to mean brightness and contrast. Taking into account the above, the following model was searched for:

$$T_{opt} = f(L_{mean}, \sigma_n). \tag{14}$$

By use of methods of nonlinear estimation, four models were tested of the overall form described by Eq. (14):

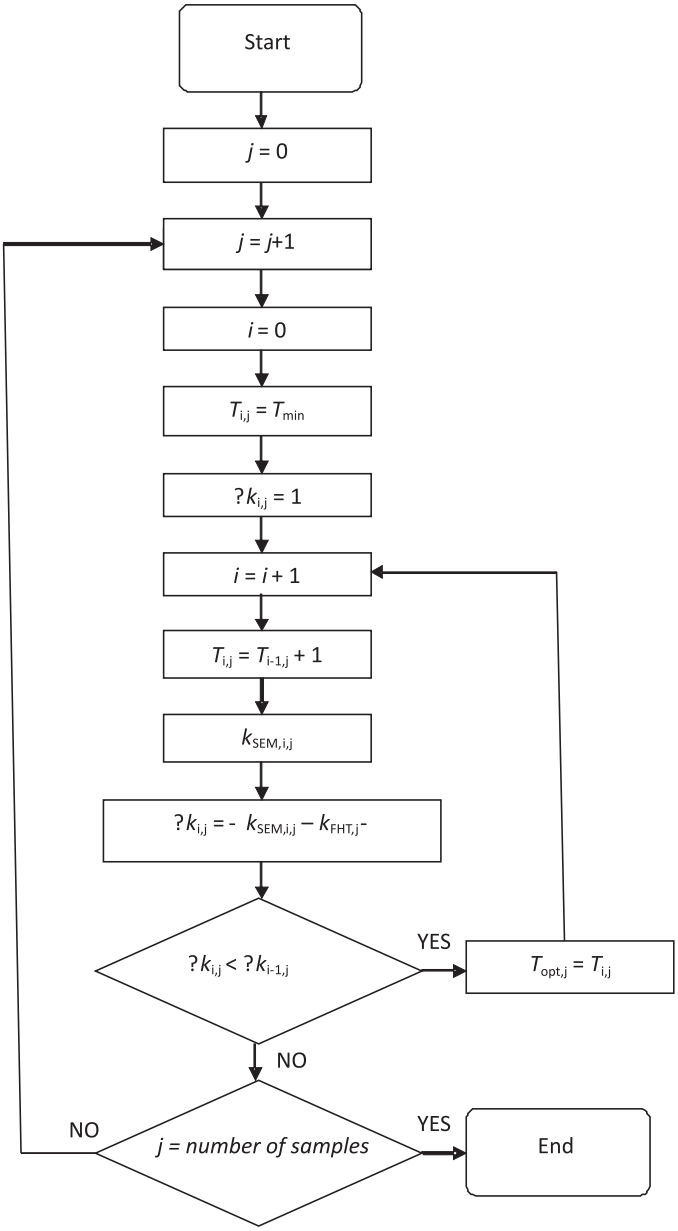

Fig. 5. The principle of the method of identification of the optimum threshold values $T_{opt,j}$ (see details in text)

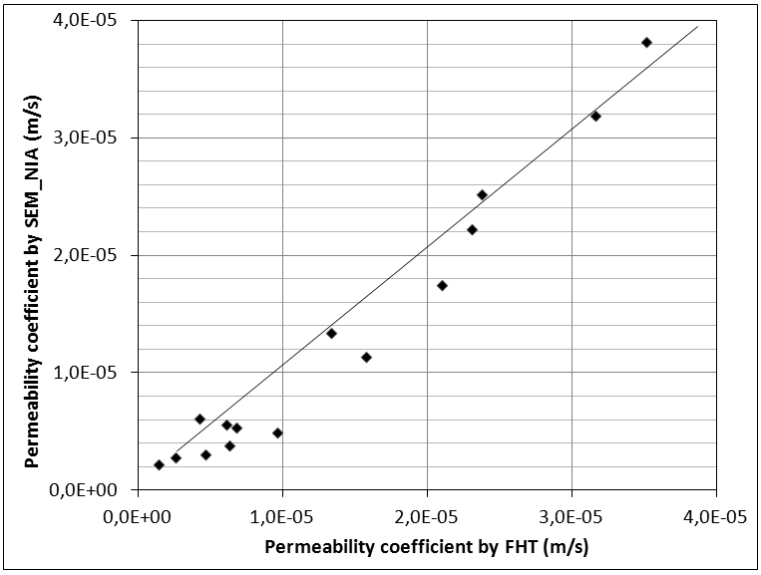

Fig. 6. The values of the permeability coefficient determined by analysis of the SEM photographs (pores identified by use of NIA) vs. the values determined by FHT

$$T_{opt} = a_1 \cdot L_{mean} + a_2 \cdot \sigma_n + a_3, \tag{15}$$

$$T_{opt} = a_1 \cdot (L_{mean})^2 + a_2 \cdot L_{mean} + a_3 \cdot (\sigma_n)^2 + a_4 \cdot \sigma_n^+ a_5, \tag{16}$$

$$\begin{aligned} T_{opt} = {} & a_1 \cdot (L_{mean})^3 + a_2 \cdot (L_{mean})^2 + a_3 \cdot L_{mean} + \\ & + a_4 \cdot (\sigma_n)^3 + a_5 \cdot (\sigma_n)^2 + a_6 \cdot \sigma_n + a_7, \end{aligned} \tag{17}$$

$$T_{opt} = a_1 \cdot (L_{mean})^{a_2} + a_3 \cdot (\sigma_n)^{a_4} + a_5. \tag{18}$$

Initially, the models were tested with all 50 samples for which SEM photographs were available (Table 1). There correlation coefficients R were 0.838, 0.863, 0.874 and 0.852 for Eqs. (15), (16), (17) and (18) respectively. Such results allow to draw the following conclusions:

1. Even the simplest linear model by Eq. (15) can be admitted to be well-fitting. This fact indirectly speaks in favor of the method of estimating the permeability coefficient on base of analyzing SEM photographs, since no correlations between the optimum threshold and image parameters would be expected if the values of T_{opt} were obtained accidentally.
2. For the polynomial models (Eqs. 15–17), the quality of the fit insignificantly depends on the degree of equation. It means that a subset of results unexplained by the models given by the general equation Eq. (14) exists in the investigated

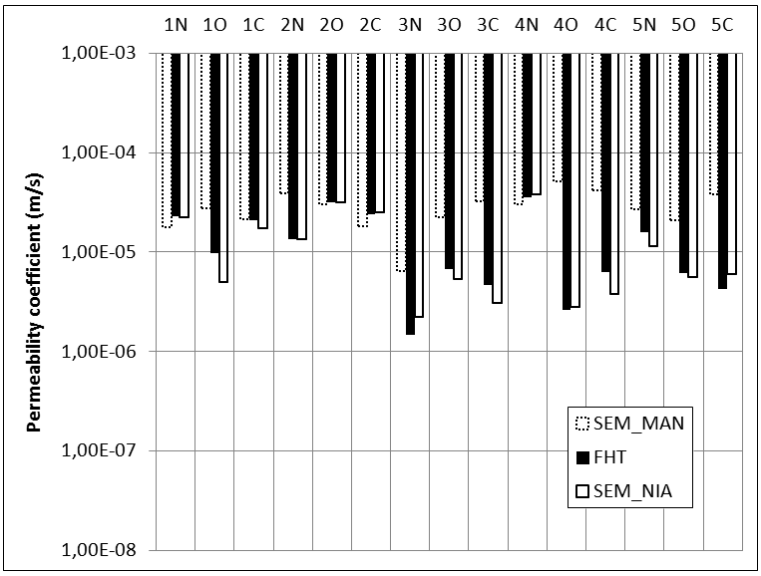

Fig. 7. Comparison of the average values of the permeability coefficient obtained by analysis of the SEM photographs (pores identified manually and by use of NIA) and the values obtained by the FHT method in five soils frozen in three freezing systems: N – non-frozen, O – open system, C – closed system

population. This could be a manifestation of a random component or factors not taken into consideration by Eq. (14).

Table 2. Parameters of models by Eqs (14)–(17)

Parameter	Model given by Eq.			
	(14)	(15)	(16)	(17)
Number of samples n	50	50	50	50
Correlation coefficient R	0.83823	0.86325	0.87432	0.85802
Proportion of variance explained	70.263	74.520	76.443	73.620
a_1	0.204969	0.074724	−0.014329	0.000000
a_2	1.634081	−7.57905	2.335432	8.659526
a_3	17.18162	0.109751	−126.102	0.002423
a_4	–	−2.12177	−0.019976	2.910325
a_5	–	249.8496	1.127440	43.07887
a_6	–	–	−18.9358	–
a_7	–	–	2404.341	–

Basing on the second conclusion, in the next variant of calculations the 6 data, for which relative error was greater than 10%, were excluded from the analysis.

The obtained results, presented in Table 2, prove a significantly better fit for all the tested models. There is an observed increase in correlation coefficient values (e.g. from $R = 0.874$ to $R = 0.948$ in the case of the best fitted model by Eq. (17)) as well as the proportion of variance explained (e.g. from 76.4% to 89.8% in the case of model by Eq. (17)). As in the case of models obtained for 50 samples, the quality of fit very slightly depends on the degree of equation.

Table 3. Parameters of models by Eqs (14)–(17) after exclusion of 6 outstanding observations

Parameter	Model given by Eq.			
	(14)	(15)	(16)	(17)
Number of samples n	44	44	44	44
Correlation coefficient R	0.93156	0.93888	0.94771	0.93853
Proportion of variance explained	86.781	88.149	89.816	88.084
a_1	0.250878	0.019805	−0.013254	0.000000
a_2	1.572983	−1.77788	2.121416	4.431165
a_3	16.45474	0.059122	−112.517	0.029007
a_4	–	−0.434701	−0.015992	2.141154
a_5	–	84.34569	0.877230	39.39121
a_6	–	–	−14.0062	–
a_7	–	–	2095.956	–

5. Conclusions

1. It has been proved that a proper description of the permeability coefficient by use of the SEM data is possible. A simplistic equation (Eq. (11)), describing the permeability coefficient of a flat segment as a function of hydraulic radius and pore area, yielded results comparable to the Falling Head Test(FHT), even when pores were identified manually. It seems that such an estimation procedure of the permeability coefficient could be useful as an alternative to the empirical equations.
2. Application of the Numerical Image Analysis (NIA) for the identification of pores on SEM photographs improves the process significantly, but a solution of the problem of thresholding is needed. The presented procedure of finding the optimum threshold T_{opt} is based on minimization of the deviation $\Delta k_{i,j}$, calculated as the absolute value of the difference between $k_{SEM,i,j}$ and $k_{FHT,j}$, i.e. the permeability coefficients determined by the SEM analysis and FHT, respectively. Since the aim of this study is to examine the possibility of using SEM as a tool for permeability coefficient determination, the optimum threshold was searched for all the samples under investigation. However, it would make

sense in all the cases, when strict identification of pores is required, e.g. analysis of microstructural parameters such as pore size distribution, pore roundness, Feret diameter, compactness and so on. Then, the values of the permeability coefficient obtained indirectly (e.g. by FHT) would only be used to determine the optimum threshold values T_{opt}, the latter allowing for the correct identification of pores and their morphometric parameters.

3. There is strong evidence that the optimum threshold values T_{opt} significantly depend on SEM image parameters. The presented statistical models, in which T_{opt} is a function of mean gray level L_{mean} and standard deviation σ_n yielded relatively high correlation coefficients. Such models could find use in cases, when only a limited number of direct measurements of the permeability coefficient *k*and optimum threshold values T_{opt} for a larger population of samples are available. After calibration of a given model by use of available data set, further values of T_{opt} could be calculated by one of the proposed equations and consequently the permeability coefficient be determined by Eq. (11). Particularly, the effect of cyclic freeze-thaw could be tested in this manner, taking data for unfrozen natural clay as a standard.

Acknowledgments

This work was partially supported by the Polish Ministry of Science under grant N N525 349538 and the Operational Program Human Capital (OP HC), contract number UDA-POKL.04.01.01-00-175/08-00.

References

Aoyama K., Ogawa S., Fukuda M. (1985) Temperature dependencies of mechanical properties of soils subjected to freezing and thawing, [in:] Kinosita S., Fukuda M. (Eds.), *Proceedings of the Fourth International Symposium on Ground Freezing, 5-7 August 1985, Sapporo, Japan*, A.A. Balkema, Rotterdam, 217–222.

Baykal G., Türe E. (1998) The effect of freeze – thaw cycles on the performance of compacted clay, [In:] *Contaminated and derelict land, The proceedings of the second international symposium on Geotechnics Related to the Environment, September 1997, Kraków, Poland*, Thomas Telford Publishing, London, 382-385.

Chamberlain E. J., Gow A. J. (1979) Effect of freezing and thawing on the permeability and structure of soils, *Engineering Geology*, **13**, 73–92.

Das, Braja M. (1985) *Principles of geotechnical engineering*, 4th ed., PWS, Boston. Czy to jeden autor o podwójnym nazwisku, czy dwaj autorzy, jeśli dwaj, to brak inicjału Dasa

Grabowska-Olszewska B. (Ed.) (1990) *Metody badań gruntów spoistych* (Methods of investigation of cohesive soils) (in Polish), Wydawnictwa Geologiczne, Warszawa.

Grabowska-Olszewska B. (Ed.) (1998) *Właściwości gruntów nienasyconych* (Properties of unsaturated soils) (in Polish), Państwowe Wydawnictwo Naukowe, Warszawa.

Hohmann-Porebska M. (2002) Microfabric effects in frozen clays in relation to geotechnical parameters, *Applied Clay Science*, **21**, 77– 87.

Kujala K., Laurinen K. (1989) Freeze–thaw effects on thaw settlement and pore pressure, [in:] *Frost in Geotechnical Engineering*, Technical Research Centre of Finland, Espoo, 523–533.

Kumor M. K. (1989) An increase in clays frost heave resulting from frost change in microstructure, [in:] *Frost in Geotechnical Engineering*, Technical Research Centre of Finland, Espoo, 535–545.

Landau L. D., Lifshitz E. M. (1987) *Fluid Mechanics*, Pergamon Press, 2nd ed.

Nagasawa T., Umeda Y. (1985) Effects of freeze–thaw process on soil structure, [in:] Kinosita S., Fukuda M. (Eds.) *Proceedings of the Fourth International Symposium on Ground Freezing, 5-7 August 1985, Sapporo, Japan*, A.A. Balkema, Rotterdam, Vol. II, 219–224.

Ogata N., Kataoka T., Komiya A. (1985) Effect of freezing–thawing on the mechanical properties of soil, [in:] Kinosita S., Fukuda M. (Eds.) *Proceedings of the Fourth International Symposium on Ground Freezing, 5-7 August 1985, Sapporo, Japan*, A.A. Balkema, Rotterdam, 201–207.

Sergeev Y. M., Spivek G. V., Sasov A. Y., Osipov V. I., Sokolov V. N. (1984) Quantitative morphological analysis in a SEM–microcomputer system – II. Morphological analysis of complex SEM images, *Journal of Microscopy*, **135**, 13–24.

Skarzynska K. (1980) Effect of freezing process on the selected properties of frost–susceptible soils, *Proceedings of the Second International Symposium on Ground Freezing, Trondheim, Norway*, 75–84.

Skarzynska K. (1985) Formation of soil structure under repeated freezing–thawing conditions, [in:] Kinosita S., Fukuda M. (Eds.) *Proceedings of the Fourth International Symposium on Ground Freezing, 5-7 August 1985, Sapporo, Japan*, A.A. Balkema, Rotterdam, Vol. II, 213–218.

Stepkowska E. T. (1977) Test sorpcyjny i możliwość jego zastosowania w różnych badaniach (Sorption test and possibilities of its use) (in Polish), *Arch. Hydrotech.*, **XXIV**, 411–420.

Stepkowska E. T., Skarzynska K. (1989) Microstructural changes in clays due to freezing, [in:] *Frost in Geotechnical Engineering*, Technical Research Centre of Finland, Espoo, 573–582.

Viklander P., Eigenbrod D. (2000) Stone movements and permeability changes in till caused by freezing and thawing, *Cold Regions Science and Technology*, **31**, 151–162.

Wang D. Y., Ma W., Niu Y. H., Chang X. X., Wen Z. (2007) Effects of cyclic freezing and thawing on mechanical properties of Qinghai–Tibet clay, *Cold Regions Science and Technology*, **48**, 34–43.

Yong R. N., Boonsinuk P., Yin C. W. P. (1985) Alteration of soil behavior after cyclic freezing and thawing, [in:] Kinosita S., Fukuda M. (Eds.) *Proceedings of the Fourth International Symposium on Ground Freezing, 5-7 August 1985, Sapporo, Japan*, A.A. Balkema, Rotterdam, 187–195.